Pea protein isolate nanocomposite films for packaging applications: Effect of starch nanocrystals on the structural, morphological, thermal, mechanical and barrier properties

Viviane Machado Azevedo, Ana Carolina Salgado de Oliveira*, Soraia Vilela Borges, Josiane Callegaro Raguzzoni, Marali Vilela Dias, Ana Letícia Rodrigues Costa

Ana Carolina Salgado de Oliveira, Food Science Department, Federal University of Lavras (UFLA), 37200-900, Lavras, MG, Brazil

ABSTRACT

Studies have been made to explore the utilization of pea proteins in terms of edible film and coating materials. The reinforcement of biopolymer films with plant-based nanocrystals has been applied in order to improve their performance properties. The objective was to evaluate the effect of the incorporation of corn starch nanocrystals (SN) (0-15%) in pea protein isolate films. Thermal analysis showed that the addition of up to 5% starch nanocrystals increased thermal stability. A 22.3% decrease was observed in water vapor permeability with the addition of SN. Increasing the SN concentration altered the arrangement of the structure to interleaved, in the matrix, as seen in transmission micrographs. This study showed that the use of corn starch nanocrystals as reinforcement in pea protein films had an effect on the films. The incorporation of up to 10% SN is suggested in order to increase the performance properties of pea protein isolate films..

Keywords: Food packaging; Nanoparticles; Thermal analysis; X-ray diffraction; Transmission electron

INTRODUCTION

The food industry uses films and other forms of packaging to store food. Food packaging is evolving in response to changing consumer demands for preserved, fresh and tasty food, as well as convenient packaging that also assists in quality control and extends shelf life (Giuffrè et al. 2019; Rizzo et al. 2018; Sicari et al. 2019). In addition to these factors, there is an advance in materials science and technology and a reduction in the use of non-biodegradable materials in the production of packaging (de Castro e Silva et al. 2020; de Oliveira et al. 2019; Rizzo et al. 2018).

The production of nanomaterials (size between 0.1 and 100 nanometers) and technologies for their incorporation into packaging are promising and there is a constant search for improvement of the properties of different biodegradable materials types to replace conventional materials with high environmental impact (Chen et al. 2004; Iwatake et al. 2008; Ma, Chang, and Yu 2008; Petersson et al. 2007;

Ferreira et al. 2018; de Castro e Silva et al. 2020). Thus, the packaging industry dependence on synthetic material would be reduced (García et al. 2011).

Starch is a semicrystalline polymer and its use is interesting for the production of nanocrystals because of its versatility, low price, biodegradability, and availability (Li et al. 2015; Savadekar and Mhaske 2012; Weerapoprasit and Prachayawarakorn 2019). Found in vegetables and stored in the form of reserve granules, it is a homopolysaccharide formed by two fractions: amylose and amylopectin. Amylose is composed of the glucose unit with α-1,4glycosidic bonds, thereby forming maltose units (linear structure). Amylopectin has the same basic structure, but it has considerably shorter chains and α-(1,6)-branches (Azevedo et al. 2017; Damodaran 2010; García et al. 2011).

Among the various existing nanomaterials, there is the recent use of starch nanocrystals to increase performance properties in biodegradable films, particularly those formed from waxy

maize starch. This material has shown effective results in different polymer matrices (Bouthegourd et al. 2011; Kristo and Biliaderis 2007; Tian and Xu 2011; Viguié et al. 2007; Zheng et al. 2009; Angellier et al. 2006; Angellier et al. 2005) due to low cost and biocompatibility in strengthening polymer properties (Le Corre et al. 2012; Angellier et al. 2004). Performance properties are also influenced by the degree of nanomaterial dispersion in the polymer chain, as they depend on the type of processing (casting or extrusion), processing variables (agitation, agitation time, temperature, presence or absence of oxygen), type and concentration of the polymeric material and type and concentration of the nanoparticles, among other variables. These properties are optimized when a high degree of exfoliation is reached, i.e., the nanoparticle dispersion occurs (Azevedo et al. 2015; Borges et al. 2013). By submitting native starch granules to acid hydrolysis, for an extended time at temperatures below the gelatinization temperature, the amorphous regions are rapidly hydrolyzed allowing separation of the crystalline lamellae, which are more resistant to hydrolysis (Kim et al. 2013; Kristo and Biliaderis 2007; Angellier et al. 2005), thus obtaining, nanoscale structures. Starch nanocrystals exhibit morphology similar to platelets. They consist of crystalline nanoplatelets, of 6-8 nm in thickness, with a length of 20-40 nm and a width of 15-30 40 nm. Thus, since at least one of the dimensions of the particles is in the nanometer scale, the term "nanoparticles" is applicable for the crystalline starch particles generated by acid hydrolysis of granular starch (Kristo and Biliaderis 2007; Angellier et al. 2005). The study of the effect of corn starch nanocrystals on pea protein isolate films is still a relatively unexplored area (Choi and Han 2002; Choi and Han 2001; Gueguen et al. 1998; Kokoszka et al. 2010).

Pea proteins represent 20% to 30% of total dry pea seeds; these proteins are mainly composed of 15% to 25% pea albumins and 60% to 70% pea globulins (Djemaoune et al. 2019; Zhou et al. 2017). Although pea protein is still dominant in the use as a food ingredient, efforts have been made to explore the utilization of pea proteins in terms of edible film and coating materials (Choi and Han 2002; Choi and Han 2001). The pea protein isolate can be used in the development of edible films with permeability to water vapor (WVP) and physical characteristics similar to those obtained from soy protein, whey protein or zein. It also has a low cost compared to other types of protein (Kokoszka et al. 2010). Protein films provide high oxygen barrier properties but have high water vapor permeability due to their hydrophilic nature (Azevedo et al. 2015; Krochta 2002; Carvalho et al. 2019; Saberi et al. 2016; dos Santos Paglione et al. 2019). This low moisture barrier can be improved by incorporating lipids (Anker et al. 2002; Chick and Hernandez 2002; Fabra et al. 2008) or reinforcing nanoparticles (Azevedo et al. 2015; Dias et al. 2014; Huneault and Li 2007).

Seeking the production of nanocomposites from renewable sources, nothing has been reported for pea protein isolate as matrix polymers. Thus, the aim of this study was to evaluate the effect of the concentration of corn starch nanocrystals in pea protein isolate films on the morphological, structural, mechanical, thermal and water vapor resistance properties.

MATERIAL AND METHODS

Material
Pea protein isolate (PPI) with 88% to 90% protein (PisaneR M9) and corn starch was obtained from Cosucra SA (Warcoing, Belgium); glycerol (GLY) and calcium chloride from Sigma-Aldrich (St. Louis, MO, USA).

Development of starch nanocrystals
The starch nanocrystals (SN) were developed with 36.73 g of starch and added to 250 mL of H_2SO_4 solution (3.16 mol L^{-1}) and stirred at 40 °C for 5 days. After stirring, the solution was neutralized with five successive washes with water and filter paper and subsequently centrifuged (Angellier et al. 2004).

Development of pea protein isolate films
The films were development according to Choi and Han (2001) and Kowalczyk and Baraniak (2011) with modifications. The control film (PPI) was obtained from 7 g (w/v) of PPI, slowly dissolving in water with stirring (500 rpm) until complete dissolution. The solution was maintained under moderate agitation (100 rpm) for 12 hours to increase hydration and complete the dissolution. Then, 3 g of glycerol (g/100g of PPI) was added and the solution was subjected to constant stirring for 10 minutes (500 rpm). The solution was heated to 90°C/20 min., cooled to room temperature, degassed (removal of bubbles) under vacuum for 1 h and 30 min. and then poured onto plexiglass plates (17 x 17 cm) at 20 g/plate. The films remained at room temperature for approximately 48 hours until complete solvent evaporation. After heating, the solution was cooled to room temperature and received a solution containing the starch nanocrystals (5; 10; 15 g/100g PPI), stirred for 10 min, warmed to 40 °C/10 min, followed by drying as in the control film (PPI). The PPI films incorporated with starch nanocrystals (SN) were developed as in the control film and coded as: SN5 (5 g·100g^{-1}PPI); SN10 (10 g·100g^{-1}PPI); SN15 (15 g·100g^{-1}PPI).

Film thickness and conditioning
The average thickness of the films was measured by reading at ten distinct points, randomly chosen in each test body, using a Mitutoyo digital micrometer (accuracy 0.01 mm Mitutoyo, Suzano, SP, Brazil). All films were stored at a controlled temperature of 23 ± 2 °C and 50 ± 5% relative humidity for 48 hours before analysis, according to the D618-00 method (ASTM 2000b).

X-Ray diffraction (XRD)

X-Ray Diffraction (XRD) was done in a diffractometer XRD-6000 (Shimadzu Corporation, Kyoto, Japan) with filter Cu (kα1) (λ = 1.5406 Å), operating with 30 kV and 30 mA. The samples were analyzed with a scanning rate of 0.02°.s⁻¹, from 4 to 60° at room temperature. The basal spacing (d) in the composites was calculated by the Bragg equation (Equation 1):

$$sen\ \theta = \lambda/2d \tag{1}$$

where: λ corresponds to the wavelength used (λ = 1.5406 Å) to generate radiation in the equipment; *d* is the distance to be calculated between crystalline planes; θ (theta) is the angle where the XRD pattern peak is detected.

Transmission electron microscopy (TEM)

Transmission electron micrographs (TEM) of the starch nanocrystals were taken with an FEI Tecnai G2 Spirit BioTWIN transmission electron microscope using an acceleration voltage of 120 kV. The films, 60 ± 10 nm thick, were cut by using a Leica EM UC6Ultramicrotome, temperature -115 to-180 °C with a Cryo 35° (Diatome) diamond knife and cutting speed of 1 mm/s. The sections were collected and placed on copper transmission grids coated with 300 mesh Lacey carbon film.

Scanning electron microscopy (SEM)

A scanning electron microscope (SEM) (LEO-EVO-40) was used to analyze films. The images were obtained under an acceleration voltage of 20 KV. The samples were placed in "stubs" with carbon tape, metalized with gold under vacuum for 180 seconds and then fixed to the microscope and photomicrographed.

Thermogravimetric analysis (TG)

The thermal stability of the films was evaluated by thermogravimetric analysis (TG) using a DTA-TG Shimadzu 60 H (Shimadzu Corporation, Kyoto, Japan), under a nitrogen atmosphere at a flow rate of 50 mL min⁻¹ with heating from room temperature to 700 °C at rate of 10 °C min⁻¹ (Lavorgna et al. 2010).

Differential scanning calorimetry (DSC)

DSC analysis was performed in a DSC TA 60 calorimeter (Shimadzu Corporation, Kyoto, Japan). The detection limit of the apparatus is 0.3 W, the sample weight was 5-6 mg and an empty capsule was used as reference. The heating and cooling ramps were fixed at 10 °C min⁻¹ and varied between -50 °C and 200 °C. The sequence used was: heating from 25 to 200 °C to eliminate the thermal history; cooling from 200 to -50 °C; and second heating to 200 °C (ASTM 1999b; ASTM 1999a). From the DSC curves, the glass transition temperature (T_g) was measured in the second heating

and the initial degradation temperature T_d (denaturation), maximum denaturation temperature (T_{max}), were evaluated in the first heating curve (Ryan et al. 2008).

Mechanical properties

The films were subjected to tensile and puncture mechanical tests using a texture analyzer (Stable Microsystems, TATX2i model, England). The tensile properties evaluated were elastic modulus (EM), tensile strength (σ_{max}) and elongation at break (E) according to the ASTM (2002) with the following parameters: 1 kN load cell and a speed of 1 mm·s⁻¹. The films were cut into 100 x 10 mm strips and fixed in the holder. The initial distance between the grips was 50 mm, with a constant separation velocity of 50 mm/min. In the puncture test, films were cut into 9 cm² pieces and fixed in an annular ring clamp (2.1 cm diameter). A spherical probe of 5.0 mm diameter was moved perpendicular to the film surface at a constant speed of 0.8 mm/s until the probe passed through the film. The properties evaluated were: Puncture strength (PS) and Puncture deformation (PD) (Azevedo et al. 2015; Chen and Lai 2008). For each sample, five replications were performed.

Water vapor permeability (WVP)

WVP analysis was conducted using ASTM (2000a). Films with 6 cm of diameter were stored at a controlled temperature of 23 ± 2 °C and 50 ± 5% relative humidity for 48 h before analysis. The films were placed in circular polymethylmethacrylate capsules (Plexiglass) with 16 to 17 g of anhydrous calcium chloride ($CaCl_2$) (0% RH), previously dried at 200 °C/2 h. The distance between the film and the $CaCl_2$ was 0.6 cm, with an exposed film area of 19.6 cm². The permeation capsules were weighed and placed in a chamber with air circulation, relative humidity (50 ± 5% RH) and controlled temperature 23 ± 2 °C in order to maintain a gradient of 50% RH through the film. A digital thermohygrometer (End Hygro, Cole Parmer) was placed in the chamber to control the relative humidity and temperature during testing. Eight weighings were done over 7 hours at half-hour intervals in three replications. The weight gain values were plotted as a function of time, and the slope calculated by linear regression ($R^2 > 0.9$). The water vapor transmission rate (WVTR, g/hr/m²) was calculated from the slope of the line divided by the exposed film area (m²). The WVP (g/(m·s·Pa)) of the film was calculated according to Equation 2:

$$W\ VP\ = \frac{(W\ VTR\ .x)}{\Delta P} \tag{2}$$

in which x is the film thickness, and ΔP is the vapor pressure difference between the faces of the film: $\Delta P = S \cdot (R_1 - R_2)$:S is the saturated vapor pressure at the test temperature (2809

kPa), R_1 is the RH of the outer side of the capsule (50%) and R_2 is the RH inside the capsule containing calcium chloride (0%).

Statistical analysis

The films were produced in triplicate. The statistical analysis was made for the mechanical properties and water-vapor permeability by Analysis of Variance (ANOVA), using Statistica software (ver. 8, Stat Soft Inc., Tulsa, USA) with significance level $p < 0.05$, and the results were compared with Tukey's test. Descriptive analyses were used to analyze data from XRD, TEM, SEM, TGA, and DSC. The curves of XRD and TGA were analyzed using the software Origin® 9.0.

RESULTS AND DISCUSSION

X-Ray diffraction (XRD)

X-ray diffraction was used to observe changes in the crystallinity of the polymer with the addition of the starch nanocrystals. Previous studies report that waxy maize starch granules have an A-type crystalline arrangement, which has two weak diffraction peaks at 10.1° and 11.5°; a peak of strong intensity at 15.3°; a double peak at 17.1° and 18.2° and a final peak of strong intensity at 23.5° (2θ) (Angellier et al. 2006; Kim et al. 2013; Cheetham et al. 1998). Corn starch nanocrystals maintain the XRD standard of waxy starch granules of native corn, typical of the A-type crystalline polymorph with sharper peaks than the native granules (Kristo and Biliaderis 2007).

Fig. 1 shows the X-ray diffraction patterns of the pea protein isolate films. The PPI film showed weak peaks indicating the presence of a crystalline and amorphous structure. Li et al. (2015) reported that PPI films presented a peak around 14° (2θ). The presence of peaks around $2\theta = 14.20$; $d = 6.24$ Å and $2\theta = 17.04$; $d = 5.21$ Å in the SN5; SN10 and SN15 films is related to the A-type diffraction peaks. The magnitude of the peaks increases with the addition of SN (5-15%), demonstrating that possibly the crystallinity of the starch nanocrystals was preserved during processing by casting (Fig. 1). Moreover, the lack of diffraction peaks at $2\theta = 10.1°$ and 11.5° and reduced high-intensity peak at 15.3° down to 14.2° may be related to possible interleaving and interaction between polymer and nanoparticle.

Transmission Electron Microscopy (TEM)

The transmission electron microscopy shows the intercalation and/or exfoliation of the SN platelets in the PPI matrix. The micrograph of PPI films; SN5; SN10 and SN15, are shown in Fig. 2.

The micrograph of the PPI film is shown in Fig. 2A. The SN5 film (Fig. 2B) showed fibrillar structures with a
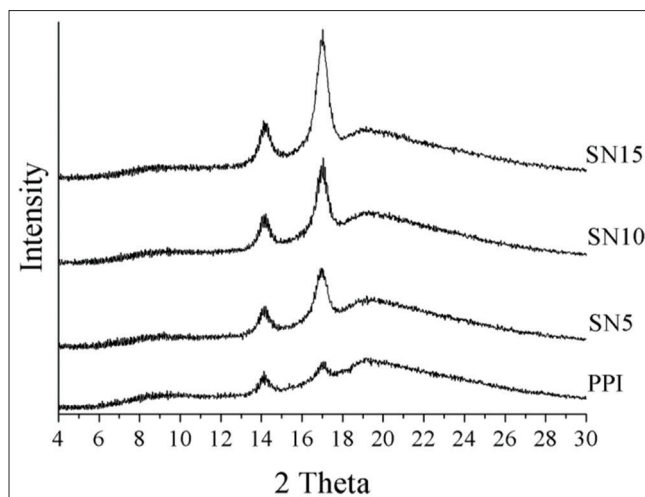

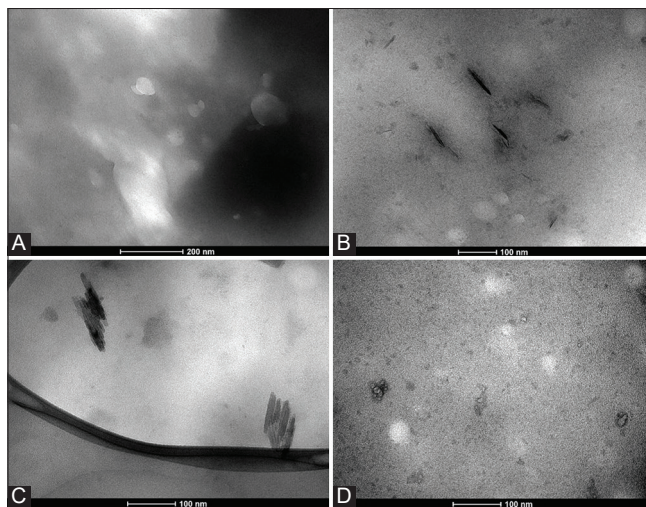**Fig 1.** XRD of PPI/SN bionanocomposites.

Fig 2. TEM micrographs of PPI/SN nanocomposites. A) PPI; B) SN5; C) SN10; D) SN15.

possible dispersion of the 210 starch nanocrystals in the PPI matrix. With the increase of the SN to 10% (Fig. 2C), the structural arrangement changed from exfoliated to intercalated (partially exfoliated). This explains the magnitude increase of the peaks with increasing SN concentration (5-15%) according to the XRD graph (Fig. 1). The addition of 15% SN to the film caused agglomeration of the starch nanocrystals characteristic of a spherical structure. Fibrillar structures are obtained from starch nanocrystals during starch hydrolysis. It is characterized by being a rigid structure with strong interfacial interaction which contributes to better mechanical performance, better barrier properties, and greater thermal resistance. However, it may also aggregate and impair the mechanical and barrier properties (Angellier et al. 2005; Kristo and Biliaderis 2007).

Scanning Electron Microscopy (SEM)

Fig. 3 presents the SEM micrographs of the PPI film surfaces. The PPI film presented rougher surfaces and

pores or cavities (Fig. 3A). Sun et al. (2013) studied the morphological properties of blends of pea starch (PS) and pea protein isolate (PPI) and found differences in the film surfaces in varying PPI/PS proportions. These authors report that the increased PPI concentration can disrupt the gel formation of the PS network and cause a phase separation.

The addition of nanocrystals caused the PPI film surfaces to become smoother and more homogeneous (Fig. 3B; 3C; 3D), however, with a possible porosity in film SN10 (Fig. 3C). We observed a regular distribution of spherical particles of different sizes for all films with SN, in which larger particles represent small particle aggregates (Fig. 3B; 3C; 3D). Liu et al. (2009) studied the size and morphology of the starch particles in a colloidal state by SEM. These

authors showed that the starch granules had spherical, micro-porous structure, bright spots and were capable of retaining large amounts of water.

Kim et al. (2013) studied the effect of ultrasonic treatment on the preparation of waxy maize starch nanoparticles, and obtained spherical nanoparticle suspensions, well defined and intact, but with a disordered crystalline arrangement. A smooth, homogeneous and fragile surface is characteristic of waxy maize starch matrix with incorporated starch nanocrystals and the absence of glycerol. There was a strong interaction between starch nanocrystals and the glycerol form fibrillar structures when incorporated in waxy maize starch matrices (García et al. 2011). Angellier et al. (2005) studied the incorporation of starch nanocrystals in natural rubber films. These authors attributed the existence of the starch nanocrystals to white points, whose concentration is a direct function of the starch content in the composite.

Thermogravimetric analysis (TG)
The thermal stability of pea protein nanocomposites and starch nanocrystals was studied by thermogravimetric analysis (TGA). Three film degradation stages in the range from 45 °C to 800 °C were observed and represented by thermogravimetric and the derivative thermogravimetric (DTG) curves (Fig. 4). The decomposition presented in the first stage occurs at about 45 to 200 °C corresponding to loss of water, volatiles and compounds of low molecular weight (Azevedo et al. 2015; García et al. 2011; Martínez-Camacho et al. 2010). The second stage is from 200 to 650 °C, corresponding to the chemical decomposition
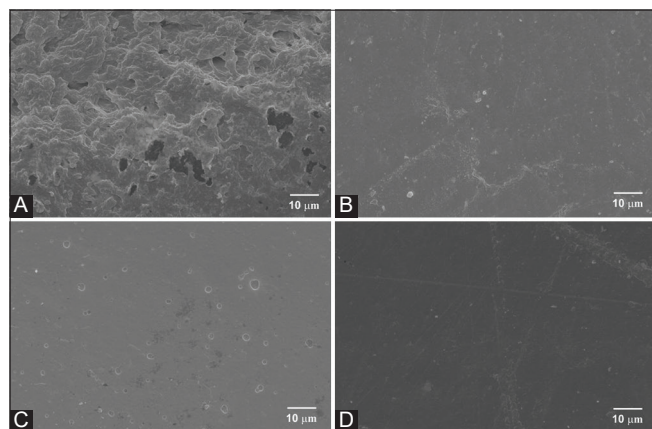

Fig 3. SEM. Surface micrographs of PPI/SN bionanocomposites. (A) PPI; (B) SN5; (C) SN10; (D) SN15.
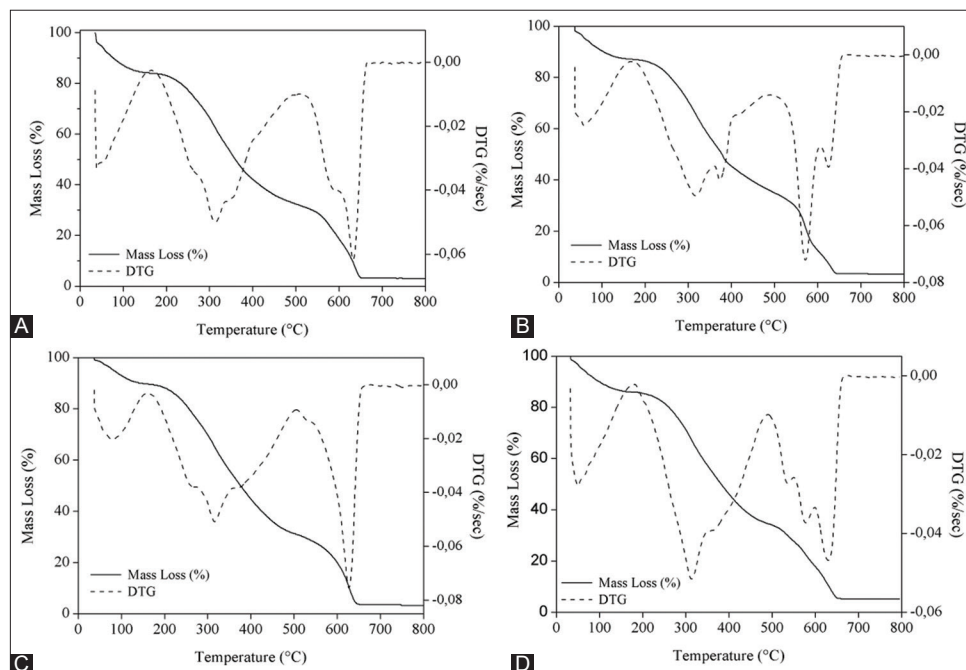

Fig 4. TGA/DTG curves. A) PPI; B) SN5; C) SN10; D) SN15.

of the components present in the films. The oxidative degradation of carbon residues formed during the second degradation stage is presented in the third stage from 650 °C to 800 °C (Fig. 4).

Table 1 presents the nanocomposite thermal stability parameters. It can be seen that the addition of starch nanocrystals increased the film degradation T_i compared to the control film (PPI) with a mass loss percentage reduction (M_{loss}) in the first and second stage. This indicates increased film stability regarding thermal decomposition (Table 1). The smaller the weight loss percentage variation range (M_{loss}), the greater the stability of the materials under thermal decomposition (Azevedo et al. 2015; Canevarolo Jr 2004). The main weight loss, between 250 and 390 °C (second stage), is attributed to the decomposition of the polymer (PPI). However, films with more than 5% of SN showed a decrease in thermal stability in T_i and T_f. This fact is attributed to the presence of large amounts of sulfate groups on the SN surface (Angellier et al. 2005; Le Corre et al. 2012), in which the SN depolymerization was catalyzed. There was an increased percentage of Res_{800} for films with SN. The presence of sulphate groups, even at low SN concentrations, cause an increase of the carbonaceous material formed in the third stage (Res_{800}), confirming that sulfate groups act as flame retardants (Roman and Winter 2004). Li et al. (2015) studied pea starch films with starch nanocrystals and reported increased thermal stability with 1; 3 and 5% SN relative to pure film.

The second and third stages showed little temperature variation in which the maximum decomposition rate ($DTG_{máx}$) occurs (Table 1). This can be attributed to strong interactions between PPI and SN. The presence of the third degradation stage corresponds to secondary reactions. In this stage, all the films containing SN their initial decomposition temperature (T) was reduced in relation to the PPI film. This results in poor thermal stability, possibly suggesting the degradation of starch nanocrystals (Table 1). At the three decomposition stages, the SN10 film showed the best thermal stability due to increase in Ti and lower M_{loss}. There are few studies reporting the interactions between proteins and starch nanocrystals and their performance properties. (Tian and Xu 2011) reported that starch nanocrystals have an affinity for proteins and little interaction between protein/glycerol. Studies with starch nanocrystals in the starch matrix have shown that the thermal decomposition of the nanocomposite also occurs in three stages and the starch nanocrystal degradation occurs above 180 °C (García et al. 2011).

Mechanical properties

Table 2 presents the average results for the mechanical properties (Elastic Modulus (EM), Tensile strength (σmax), Elongation at break (E), Puncture strength (PS) and Puncture deformation (PD)) of PPI/SN nanocomposites. The films showed no significant difference regarding the tensile strength property, i.e., the force required to break the film is about the same for all treatments. The addition of 15% SN made the film less rigid and weaker than the other treatments. This indicates greater interaction between the nanoparticles and consequently greater agglomeration and elastic modulus reduction. This result reinforces the evidence on the transmission micrographs (Fig. 2D), in which we observed SN nanoparticles agglomeration at the concentration of 15%. In addition, films incorporated

Table 1: Thermal stability, obtained by TGA, of PPI/SN nanocomposites in the 1st, 2nd and 3rd stages of degradation

First stage			
Film (g.100g^{-1} PPI)	T_i (°C)[b]	DTG (%/sec)	T_f (°C)	(%) M_{loss} (T_i -T_f)
PPI	48.12	77.96	85.93	12.99
SN5	51.96	49.96	69.78	10.25
SN10	67.69	-	101.2	7.86
SN15	49.73	58.75	96.79	10.24
Second stage			
Film (g.100g^{-1} PPI)	T_i (°C)[b]	DTG (%/sec)	T_f (°C)	(%) M_{loss} (T_i -T_f)
PPI	248.4	315.9	389.4	61.1
SN5	266.89	312.87	391.19	51.13
SN10	254.3	313.7	345.95	54.63
SN15	254.17	316.46	348.36	55.13
Third stage			
Film (g.100g^{-1} PPI)	T_i (°C)[b]	DTG_{max} (°C)	T_f (°C)	M_{loss} (%) (T_i -T_f)	$Res_{800 °C}$ (%)
PPI	599.14	627.38	639.13	23.84	3,78
SN5	565.26	629.87	648.17	27.92	5,48
SN10	596.66	633.14	648.07	24.94	4,31
SN15	554.85	571.64	613.69	27.52	4,05

*T_i (initial decomposition temperature); DTGmax (maximum decomposition temperature); T_f (final decomposition temperature); M_{loss} (mass loss percentage in the decomposition range); Res800°C (percentage of residue at 800 °C)

500

Emir. J. Food Agric ● Vol 32 ● Issue 7 ● 2020

Table 2: Elastic Modulus (EM), Tensile strength (σ_{max}), Elongation at break (E), Puncture strength (PS) and Puncture deformation (PD) of PPI/SN nanocomposites

Film (g.100g^{-1} PPI)	Elastic Modulus (EM) (MPa)	σ_{max} (MPa)	Elongation at break (E) (%)	Puncture strength (PS) (N)	Puncture deformation (PD) (mm)
PPI	25.40±2.6[a]	1.95±0.24[ab]	168.87±0.18[a]	4.10±0.30[a]	6.03±0.17[a]
SN5	24.65±4.5[a]	2.08±0.30[b]	172.29±0.34[ab]	5.12±0.60[ab]	6.05±0.35[a]
SN10	25.47±4.2[a]	2.14±0.25[b]	194.17±0.18[b]	4.71±0.95[ab]	5.59±0.52[a]
SN15	16.09±3.9[b]	1.72±0.20[a]	203.17±0.11[b]	3.48±0.06[b]	5.77±0.10[a]

* Means observed in the column with the same letter do not differ statistically (p< 0.05)

with higher SN concentrations (10 and 15%) tend to stretch more until rupture (E) compared to films with low concentrations. This result reinforces the evidence on the transmission micrographs (Fig. 2D), in which we observed SN nanoparticle agglomeration.

The tensile strength and puncture values may be used as a measure of filmhardness (Park and Zhao 2004; Azevedo et al. 2015). There was a reduction of PS for the SN15 film in relation to the PPI film. This indicates that the film became weaker and a low vertical force is required for puncture. Agglomeration of the starch nanocrystals, for SN15, as reported in the TEM micrographs, possibly hindered the mobility of the polymer matrix, resulting in less resistant and more elastic films. Angellier et al. (2005) reported that a regular distribution of cellulose nanocrystals in the polymer matrix is essential to obtain better mechanical properties.

Li et al. (2015) studied mechanical properties of starch nanocrystals (SNCs) in reinforced pea starch films. The authors concluded that the tensile strength and Young's modulus values of the films decreased and the elongation at break values increased with the addition of 5-9% SNCs compared to the pure pea starch film. These authors attribute this result to the large number of hydroxyl groups on the surface of the SNCs, which led to the formation of bonds among the nanocrystals.

Zheng et al. (2009) incorporated pea starch nanocrystals in a soybean protein isolate matrix. The pea starch nanocrystals showed the predominant reinforcing function at low concentrations (< 2% wt%), resulting in increased strength and Young's modulus. These authors report that the increase in mechanical properties was attributed to uniform dispersion of pea starch nanocrystals in the amorphous region of the soy protein isolate matrix. Furthermore, these authors reported that the increase in the concentration of pea starch nanocrystals causes a strong tendency towards nanocrystal self-aggregation.

Differential scanning calorimetry (DSC)

The effect of the SN on PPI films were analyzed by DSC and are shown in Table 3. The addition of SN caused alterations in the initial denaturation temperature (T_d). The T_d increased with the addition of 5% SN when compared

Table 3: WVP and DSC of PPI/SN nanocomposites

Films (g·100g^{-1})	WVP (× 10^{-6}) (g.m^{-1}.s^{-1}.Pa)	T_d (°C)[a]	T_{max}	T_g (°C)
PPI	3.60 ±9.3.10^{-8} [a]	60.82	79.87	132.86
SN5	2.77 ±9.4.10^{-8} [b]	65.84	80.02	116.8
SN10	2.79 ±3.6.10^{-7} [b]	62.92	79.13	112.42
SN15	3.07 ±1.2.10^{-7} [c]	60.43	77.69	99.64

* Means observed in the column with the same letter do not differ statistically (p < 0.05). [a]Abbreviations: T_d, initial degradation temperature (denaturation); T_{max}, maximum degradation temperature; T_g, glass transition temperature

to control film (PPI) (Table 3). The increase in denaturation temperature might indicate that the addition of SN can further reduce the mobility of the polymer chains and enhance the thermal stability. However, SN10 and SN15 films show a decrease of T_d compared to the film SN5. This reduction is associated to lower thermal stability of the films caused by the possible nanoparticle agglomerates in the PPI matrix. The addition of SN was not sufficient to increase T_{max}. Kokoszka et al. (2010) studied the effect of different concentrations of whey protein isolate and glycerol and found T_d values between 60.6 and 72.5 °C and those of Tmax from 68.7 to 77.1 °C. Azevedo et al. (2015) reported denaturation temperatures (T_d and T_{max}) in whey protein isolate films with montmorillonite clay nanoparticles between 58.95 to 68.13°C (T_d) and 64.41 to 79.01 °C (T_{max}).

The beginning of polymer chain movement passing from the glassy state (more ordered molecules) to the rubbery state (more flexible and less ordered) is called the glass transition temperature (T_g) (Azevedo et al. 2015; Canevarolo Jr 2004). The control film (PPI) T_g was 132.86 °C (Table 3). Adding SN decreased the T_g of the films compared to the PPI film. The T_g decrease can be attributed to the presence of water in the SN nanoparticles which causes a plasticizing effect, reducing the T_g. Water has a plasticizing effect, increasing the mobility of the polymer chain and decreasing the thermal stability of the nanocomposites (Canevarolo Jr 2004). In addition, as reported in mechanical properties, the SN15 film showed lower EM, i.e., lower stiffness and, consequently, a decrease in T_g.

Water vapor permeability (WVP)

Table 3 shows how the WVP of nanocomposites (PPI/SN) varied with the different concentrations of cellulose

nanocrystals. With the addition of SN the PPI film showed a WVP reduction with up to 10% SN (Table 3).

This represents an improvement of barrier properties of the nanocomposite which can be attributed to a possible SN interleaving/dispersion of throughout the PPI matrix, as seen in transmission micrographs for SN5 and SN10 films. This tendency has been explained by the increased winding path promoted by the nanoparticles and presented in several studies. Factors such as polymer chain mobility and specific interaction between polymer functional groups also produce effects on the WVP (García et al. 2000; Li et al. 2015; Salvador-Figueroa et al. 2017). Shi et al. (2013) reported that starch nanocrystals could have easily been dispersed throughout starch film matrices, leading to a winding course for the mobility of water molecules and consequent decrease in WVP. A longer water molecule diffusion path reduces the permeability to water vapor (Li et al. 2015; Sinha Ray and Okamoto 2003). However, the SN15 film presented increased WVP. This is attributed to nanoparticle agglomeration, as seen in the TEM micrographs (Fig. 2D) and SN crystallinity due to increasing concentration (15%) and the consequent difficulty of water molecule migration through the film. Müller et al.(2011), studied starch films and found that the addition of up to 5% SN lessens film water resistance, possibly due to SN aggregation.

CONCLUSION

There are few studies that have investigated the effect of corn starch nanocrystals on plant source protein films. This study showed that the use of corn starch nanocrystals as reinforcement in pea protein films had an effect on the performance properties of the films produced by casting. The SEM and TEM micrographs confirmed that the starch nanocrystals were uniformly distributed in the PPI matrix with up to 10% SN. The incorporation of SN up to 10%, reduced water vapor permeability, mechanical properties and increased thermal stability of the films. Thus, the incorporation of up to 10% SN is suggested in order to increase the performance properties of pea protein isolate films.

ACKNOWLEDGMENTS

Authors' contributions
The authors Josiane Callegaro Raguzzoni and Soraia Vilela Borges were responsible for structuring the project and revising the text of the manuscript. The authors Ana Letícia Rodrigues Costa Lelis and Marali Vilela Dias were responsible for carrying out the experiment. The authors Viviane Machado Azevedo and Ana Carolina Salgado de Oliveira were responsible for analyzing the data and writing the manuscript.

REFERENCES

Angellier, H., L. Choisnard, S. Molina-Boisseau, P. Ozil and A. Dufresne. 2004. Optimization of the preparation of aqueous suspensions of Waxy Maize starch nanocrystals using a response surface methodology. Biomacromolecules. 5: 1545-51.

Angellier, H., S. Molina-Boisseau, P. Dole and A. Dufresne. 2006. Thermoplastic Starch-Waxy maize starch nanocrystals nanocomposites. Biomacromolecules. 7: 531-39.

Angellier, H., S. Molina-Boisseau, L. Lebrun and A. Dufresne. 2005. Processing and structural properties of Waxy Maize starch nanocrystals reinforced natural rubber. Macromolecules. 38: 3783-92.

Anker, M., J. Berntsen, A. M. Hermansson and M. Stading. 2002. Improved water vapor barrier of whey protein films by addition of an acetylated monoglyceride. Innovative Food Sci. Emerg. Technol. 3: 81-92.

ASTM. 1999a. Standard Test Method for Transition Temperatures of Polymers by Differential Scanning Calorimetry. Philadelphia, United States of America.

ASTM. 2000a. Standard Test Method for Water Vapor Transmission of Materials. E 96-00. Philadelphia, United States of America.

ASTM. 2000b. D618, Standard Practice for Conditioning Plastics for Testing. West Coshoshocken, United States of America.

ASTM. 2002. Standard Test Method for Tensile Properties of thin Plastic Sheeting. Philadelphia, United States of America.

ASTM. 1999b. D3417, Enthalpies of Fusion and Crystallization of Polymers by Differential Scanning Calorimetry. Philadelphia, United States of America.

Azevedo, V. M., M. V. Dias, S. B. Borges, A. L. R. Costa, E. K. Silva, E. A. A. Medeiros and N. F. F. Soares. 2015. Development of whey protein isolate bio-nanocomposites: Effect of montmorillonite and citric acid on structural, thermal, morphological and mechanical properties. Food Hydrocoll. 48: 179-88.

Azevedo, V. M., S. V. Borges, J. M. Marconcini, M. I. Yoshida, A. R. S. Neto, T. C. Pereiraand C. F. G. Pereira. 2017. Effect of replacement of corn starch by whey protein isolate in biodegradable film blends obtained by extrusion. Carbohydr. Polym. 157: 971-80.

Azevedo, V. M., E. K. Silva, C. F. G. Pereira, J. M. G. Costa and S. V. Borges. 2015. Whey protein isolate biodegradable films: Influence of the citric acid and montmorillonite clay nanoparticles on the physical properties. Food Hydrocoll. 43: 252-58.

Borges, S. V., M. L. Dias, V. J. R. Pita, C. Azuma and M. V. Dias. 2013. Water vapor permeability and tensile properties of poly(l-lactic acid)/synthetic mica nanocomposites prepared by melt blending. J. Plastic Film Sheeting. 29: 112-26.

Bouthegourd, E., K. R. Rajisha, N. Kalarical, J. M. Saiter and S. Thomas. 2011. Natural rubber latex/potato starch nanocrystal nanocomposites: Correlation morphology/electrical properties. Mater. Lett. 65: 3615-17.

Canevarolo, S. V. Jr. 2004. Técnicas de Caracterização de Polímeros. Artliber, São Paulo.

Carvalho, R. A., A. C. S. Oliveira,T. A. Santos, M. V. Dias, M. I. Yoshida and S. V. Borges. 2019. WPI and cellulose nanofibres bio-nanocomposites: Effect of thyme essential oil on the morphological, mechanical, barrier and optical properties. J. Polym. Environ. 28: 231-241.

Cheetham, N. W. H. and L. Tao. 1998. Variation in crystalline type with amylose content in maize starch granules: An X-ray powder diffraction study. Carbohydr. Polym. 36: 277-84.

Chen, C. H. and L. S. Lai. 2008. Mechanical and water vapor barrier properties of tapioca starch/decolorized hsian-tsao leaf gum films in the presence of plasticizer. Food Hydrocoll. 22: 1584-1595.

Chen, G. X., G. J. Hao, T. Y. Guo, M. D. Song and B. H. Zhang. 2004. Crystallization kinetics of poly(3-hydroxybutyrate-co-3-hydroxyvalerate)/clay nanocomposites. J. Appl. Polym. Sci. 93: 655-661.

Chick, J. and R. J. Hernandez. 2002. Physical, thermal, and barrier characterization of casein-wax-based edible films. J. Food Sci. 67: 1073-1079.

Choi, W. S. and J. H. Han. 2002. Film-forming mechanism and heat denaturation effects on the physical and chemical properties of pea-protein-isolate edible films. J. Food Sci. 67: 1399-1406.

Choi, W. S. and J. H. Han. 2001. Physical and mechanical properties of pea-protein-based edible films. J. Food Sci. 66: 319-322.

Damodaran, P. 2010. KL; Fennema, OR Química de Alimentos de Fennema. 4th ed. Editora Artmed SA, São Paulo.

de Castro e Silva, P., A. C. S. Oliveira, L. A. S. Pereira, M. Valquíria, G. R. Carvalho, K. W. E. Miranda, J. M. Marconcini and J. E. Oliveira. 2020. Development of bionanocomposites of pectin and nanoemulsions of carnauba wax and neem oil pectin/carnauba wax/neem oil composites. Polym. Composites. 41: 858-870.

de Oliveira, A. C. S., J. C. Ugucioni, R. A. Rocha and S. V. Borges. 2019. Development of whey protein isolate/polyaniline smart packaging: Morphological, structural, thermal, and electrical properties. J. Appl. Polym. Sci. 136: 47316.

Dias, M. V., V. M. Azevedo, S. V. Borges, N. F. F. Soares, R. V. B. Fernandes, J. J. Marques and E. A. A. Medeiros. 2014. Development of chitosan/montmorillonite nanocomposites with encapsulated α-tocopherol. Food Chem. 165: 323-329.

Djemaoune, Y., E. Cases and R. Saurel. 2019. The effect of high-pressure microfluidization treatment on the foaming properties of pea albumin aggregates. J. Food Sci. 84: 2242-2249.

dos Santos Paglione, I., M. V. Galindo, K. C. de Souza, F. Yamashita, C. R. F. Grosso, L. S. Sakanaka and M. A. Shirai. 2019. Optimization of the conditions for producing soy protein isolate films. Emir. J. Food Agric. 31: 297-303.

Fabra, M. J., P. Talens and A. Chiralt. 2008. Tensile properties and water vapor permeability of sodium caseinate films containing oleic acid-beeswax mixtures. J. Food Eng. 85: 393-400.

Ferreira, F. V., I. F. Pinheiro, R. F. Gouveia, G. P. Thim and L. M. F. Lona. 2018. Functionalized cellulose nanocrystals as reinforcement in biodegradable polymer nanocomposites. Polym. Composites. 39: E9-E29.

García, M. A., M. N. Martino and N. E. Zaritzky. 2000. Lipid addition to improve barrier properties of edible starch-based films and coatings. J. Food Sci. 65: 941-944.

García, N. L., L. Ribba, A. Dufresne, M. Aranguren and S. Goyanes. 2011. Effect of glycerol on the morphology of nanocomposites made from thermoplastic starch and starch nanocrystals. Carbohydr. Polym. 84: 203-210.

Giuffrè, A. M., L. Louadj, P. Rizzo, E. Salvo and V. Sicari. 2019. The influence of film and storage on the phenolic and antioxidant properties of red raspberries (*Rubus idaeus* L.) cv. Erika.

Antioxidants. 8: 254.

Gueguen, J., G. Viroben, P. Noireaux and M. Subirade. 1998. Influence of plasticizers and treatments on the properties of films from pea proteins. Ind. Crops Prod. 7: 149-57.

Huneault, M. A. and H. Li. 2007. Morphology and properties of compatibilized polylactide/thermoplastic starch blends. Polymer. 48: 270-280.

Iwatake, A., M. Nogi and H. Yano. 2008. Cellulose nanofiber-reinforced polylactic acid. Compos. Sci. Technol. 68: 2103-2106.

Kim, H. Y., J. A. Han, D. K. Kweon, J. D. Park and S. T. Lim. 2013. Effect of ultrasonic treatments on nanoparticle preparation of acid-hydrolyzed waxy maize starch. Carbohydr. Polym. 93: 582-588.

Kokoszka, S., F. Debeaufort, A. Lenart and A. Voilley. 2010. Water vapour permeability, thermal and wetting properties of whey protein isolate based edible films. Int. Dairy J. 20: 53-60.

Kowalczyk, D. and B. Baraniak. 2011. Effects of plasticizers, pH and heating of film-forming solution on the properties of pea protein isolate films. J. Food Eng. 105: 295-305.

Kristo, E. and C. G. Biliaderis. 2007. Physical properties of starch nanocrystal-reinforced pullulan films. Carbohydr. Polym. 68: 146-158.

Krochta, J. M. 2002. Proteins as raw materials for films and coatings: Definitions, current status, and opportunities. Protein Based Films Coatings. 1: 1-40.

Lavorgna, M., F. Piscitelli, P. Mangiacapra and G. G. Buonocore. 2010. Study of the combined effect of both clay and glycerol plasticizer on the properties of chitosan films. Carbohydr. Polym. 82: 291-298.

Le Corre, D., J. Bras, L. Choisnard and A. Dufresne. 2012. Optimization of the batch preparation of starch nanocrystals to reach daily time-scale. Starch Stärke. 64: 489-496.

Li, X., C. Qiu, N. Ji, C. Sun, L. Xiong and Q. Sun. 2015. Mechanical, barrier and morphological properties of starch nanocrystals-reinforced pea starch films. Carbohydr. Polym. 121: 155-162.

Liu, D., Q. Wu, H. Chen and P. R. Chang. 2009. Transitional properties of starch colloid with particle size reduction from micro to nanometer. J. Colloid Interface Sci. 339: 117-124.

Ma, X., P. R. Chang and J. Yu. 2008. Properties of biodegradable thermoplastic pea starch/carboxymethyl cellulose and pea starch/microcrystalline cellulose composites. Carbohydr. Polym. 72: 369-375.

Martínez-Camacho, A. P., M. O. Cortez-Rocha, J. M. Ezquerra-Brauer, A. Z. Graciano-Verdugo, F. Rodriguez-Félix, M. M. Castillo-Ortega, M. S. Yépiz-Gómez and M. Plascencia-Jatomea. 2010. Chitosan composite films: Thermal, structural, mechanical and antifungal properties. Carbohydr. Polym. 82: 305-315.

Müller, C. M. O., J. B. Laurindo and F. Yamashita. 2011. Effect of nanoclay incorporation method on mechanical and water vapor barrier properties of starch-based films. Ind. Crops Prod. 33: 605-610.

Park, S. and Y. Zhao. 2004. Incorporation of a high concentration of mineral or vitamin into chitosan-based films. J. Agric. Food Chem. 52: 1933-1939.

Petersson, L., I. Kvien and K. Oksman. 2007. Structure and thermal properties of poly(lactic acid)/cellulose whiskers nanocomposite materials. Compos. Sci. Technol. 67: 2535-2544.

Rizzo, P., A. Cozzolino, A. R. Albunia, A. M. Giuffrè, V. Sicari, L. D. Maio, C. Daniel, V. Venditto, M. Galimberti and G. Mensitieri. 2018. Packaging technology for improving shelf-life of fruits based on a nanoporous-crystalline polymer. J. Appl. Polym. Sci. 135: 46256.

Roman, M. and W. T. Winter. 2004. Effect of sulfate groups from sulfuric acid hydrolysis on the thermal degradation behavior of bacterial cellulose. Biomacromolecules. 5: 1671-1677.

Ryan, M., E. McEvoy, S. Duignan, C. Crowley, M. Fenelon, D. M. O'Callaghan. and R. J. FitzGerald. 2008. Thermal stability of soy protein isolate and hydrolysate ingredients. Food Chem. 108: 503-510.

Saberi, B., Q. V. Vuong, S. Chockchaisawasdee, J. B. Golding, C. J. Scarlett and E. C. Stathopoulos. 2016. Mechanical and physical properties of pea starch edible films in the presence of glycerol. J. Food Proc. Preserv. 40: 1339-1351.

Salvador-Figueroa, M., D. Castillo-López, L. Adriano-Anaya, D. Gálvez-López, R. Rosas-Quijano and A. Vázquez-Ovando. 2017. Chitosan composite films: Physicochemical characterization and their use as coating in papaya Maradol stored at room temperature. Emir. J. Food Agric. 29: 779-791.

Savadekar, N. R. and S. T. Mhaske. 2012. Synthesis of nano cellulose fibers and effect on thermoplastics starch based films. Carbohydr. Polym. 89: 146-151.

Shi, A., L. Wang, D. Li and B. Adhikari. 2013. Characterization of starch films containing starch nanoparticles: Part 1: Physical and mechanical properties. Carbohydr. Polym. 96: 593-601.

Sicari, V., T. M. Pellicanò, A. M. Giuffrè, M. R. Loizzo and M. Poiana. 2019. Effect of packaging materials on the quality of kiwifruits (*Actinidia deliciosa* cv. Hayward). J. Food Meas. Charact. 13: 3033-3039.

Sinha, R. S. and M. Okamoto. 2003. Polymer/layered silicate nanocomposites: A review from preparation to processing. Prog. Polym. Sci. 28: 1539-1641.

Sun, Q., C. Sun and L. Xiong. 2013. Mechanical, barrier and morphological properties of pea starch and peanut protein isolate blend films. Carbohydr. Polym. 98: 630-637.

Tian, H. and G. Xu. 2011. Processing and characterization of glycerol-plasticized soy protein plastics reinforced with citric acid-modified starch nanoparticles. J. Polym. Environ. 19: 582-588.

Viguié, J., S. Molina-Boisseau and A. Dufresne. 2007. Processing and characterization of waxy maize starch films plasticized by sorbitol and reinforced with starch nanocrystals. Macromol. Biosci. 7: 1206-1216.

Weerapoprasit, C. and J. Prachayawarakorn. 2019. Effects of polymethacrylamide-grafted branch on mechanical performances, hydrophilicity, and biodegradability of thermoplastic starch film. Starch Stärke. 71: 1900068.

Zheng, H., F. Ai, P. R. Chang, J. Huang and A. Dufresne. 2009. Structure and properties of starch nanocrystal-reinforced soy protein plastics. Polym. Composites. 30: 474-480.

Zhou, Q. C., N. Liu and C. X. Feng. 2017. Research on the effect of papain co-extrusion on pea protein and enzymolysis antioxidant peptides. J. Food Proc. Preserv. 41: e13301.